ARTICLE

JAAS
www.rsc.org/jaas

Particle size distributions and compositions of aerosols produced by near-IR femto- and nanosecond laser ablation of brass

J. Koch,* A. von Bohlen, R. Hergenröder and K. Niemax

Institute of Spectrochemistry and Applied Spectroscopy (ISAS), Bunsen-Kirchhoff-Strasse 11, D-44139 Dortmund, Germany. E-mail: koch@isas-dortmund.de (J. Koch); Fax: +49-231-1392-120; Tel: +49-231-1392-175

Received 29th August 2003, Accepted 28th October 2003
First published as an Advance Article on the web 13th January 2004

Particle size distributions and compositions of primary aerosols produced by means of near-IR femtosecond laser ablation (λ = 775 nm) of brass in He or Ar at atmospheric pressure have been measured. Aerosols were characterized using a 13-stage low-pressure impactor covering a size range from 5 nm up to 5 μm and subsequently analyzed applying total reflection X-ray fluorescence spectrometry. The results indicate, that for femtosecond laser ablation in the low-fluence regime (<5 J cm^{-2}) ultra-fine aerosols (mean diameter $d_p \approx$ 10 nm/peak width $w_p \approx$ 35 nm) are produced. Furthermore, the total Cu/Zn ratio of these aerosols corresponds to the composition of the bulk material. In contrast, ablation above 10 J cm^{-2} results in the formation of polydisperse, bimodal aerosols, which are distributed around $d_{p1} \approx$ 20 nm ($w_{p1} \approx$ 50 nm) and $d_{p2} \approx$ 1 μm ($w_{p2} \approx$ 5 μm), respectively, and whose total Cu/Zn ratio slightly deviates from the bulk composition. In order to examine the influence of pulse duration on particle size distribution and aerosol composition, comparative measurements by means of near-IR nanosecond ablation were also performed. The data show that nanosecond ablation generally leads to an intensified formation of particles in the micrometer range. Moreover, the composition of these aerosols strongly departs from the stoichiometry of the bulk. Aspects concerning the formation of particles during ablation as well as implications for the element-selective analysis by inductively coupled plasma spectrometry are discussed.

1 Introduction

Due to its versatility and inherent sensitivity laser ablation inductively coupled plasma (LA-ICP) spectrometry certainly represents one of the most attractive methods for the spatially resolved analysis of solid states.[1] Nevertheless, the future prospects of LA-ICP spectrometry as a standard method for quantitative analysis remain uncertain since there still exists a substantial lack of appropriate reference materials, making non-matrix matched analyses necessary.[2–4] As a consequence, matrix-dependent fractionation of major and minor components can occur, which strongly affects the accuracy of experimental results achieved.

Several calibration strategies, predominantly resting on the supplemental introduction of dispersed liquid standards have been developed during recent years in order to compensate this lack.[5,6] Although these strategies lead to an increase in flexibility of LA-ICP spectrometry, they have been found being less effective for reducing fractionation.[4] It is therefore obvious, that the further development of LA-ICP-MS/OES will mainly be associated with the question to what extent elemental fractionation can be suppressed rather than improving other performance characteristics such as acquisition speed, mass resolution, or methodical sensitivity.

For instance, the analysis of metals using nanosecond LA has been found to be extremely difficult due to the inherent complexity of fractionation involving laser-, transport- and ICP-induced phenomena.[7,8] Laser-induced fractionation refers to the formation of non-stoichiometric aerosol particles during the ablation process, whereas transport-induced fractionation originates from selective particle deposition during the transport due to diffusion, gravitational settling and inertial deposition. In contrast, ICP-induced fractionation occurs whenever transported particles are not completely atomised within the ICP. As a result preferential vaporization of volatile compounds affects the accuracy of analysis. Since both particle deposition and vaporization critically depend on the mass and the particle size distribution of the primary aerosols, transport- and ICP-induced phenomena are strongly correlated.

In order to conceive appropriate strategies for the suppression of fractionation, it is important to examine these effects in a quantitative way. Even though there already exists extensive material on fractionation in LA-ICP spectrometry arrangements operated under different conditions, less effort has been invested to study its different origins. Thus, published papers usually address over-all fractionation, revealing less insight into basic mechanisms, which would be essential in order to develop strategies for suppression. In addition, reliable data concerning the influence of ultra-short pulses on fractionation are also limited,[9] while comparative studies involving extreme time regimes, *i.e.* nano- as well as femtosecond LA have not been performed at all.

First investigations addressing the separation and quantification of laser- and transport-induced fractionation were documented by Outridge *et al.*[10] It was found that for both metallic and dielectric aerosols, laser-induced effects generally govern the over-all fractionation, while ICP-induced phenomena can be neglected. However, the authors restricted their investigations on the analysis of aerosol particles produced by nanosecond LA using near-IR radiation at 1064 nm. In contrast, Guillong and Günther[11] indicate that incomplete vaporization within the ICP generally represents the main source of fractionation. They demonstrated that the cut-off diameter for incomplete vaporization of dielectric particles (glass) is of the order of 0.5 μm provided that the ICP is operated under standard conditions. However, for metallic aerosol particles the cut-off diameter should be smaller because the material-specific evaporation enthalpy, which basically determines the thermal durability, is significantly lower in most cases.

The present article reports on the characterization of brass aerosols produced by near-IR femto- and nanosecond LA

DOI: 10.1039/b310512a

under atmospheric conditions applying He or Ar as carrier gas. For this purpose, particle size distributions and compositions were determined using low-pressure impaction and total reflection X-ray fluorescence (TXRF). To study the intensity of elemental fractionation during ablation, brass was chosen as target since the volatilities of its constituents, Cu and Zn, strongly differ.

2 Experimental

2.1 Aerosol production and cell design

The experimental arrangement for aerosol classification is schematically shown in Fig. 1. Nano- as well as femtosecond pulses were generated using a CPA-type Ti:Sa laser system (CPA-10, pulse duration 170 fs, Clarc-MXR Inc., MI, USA) emitting at a wavelength of 775 nm. The laser beam was delivered to a lens (f = 100 mm) by a set of high-reflecting, dielectric mirrors and subsequently focused onto the surface of a brass sample (60.5% Cu and 39.5% Zn, Wieland Werke AG, Ulm, Germany), positioned in the centre of a cylindrical ablation cell (V = 20 cm^3). The outlet of the cell was directly mounted on the top of the impactor unit.

In order to collect a sufficient amount of material for analysis, a series of 50 craters was shot each run. Laser repetition rate and exposure time per spot were set to 10 Hz and 30 s, respectively, resulting in 300 shots per crater. Thus, 1.5×10^4 shots were applied altogether. The lateral position of the brass sample was manipulated from the outside using a pair of micrometer screws, which were integrated in the bottom of the ablation cell.

Aerosol particles were produced under He or Ar at atmospheric pressure using both nano- and femtosecond pulses. A flow rate of 1 L min^{-1} was applied to the inlet of the ablation cell. The fluence was varied by means of beam defocusing applying pulse energies of 300 μJ. The spot size at the sample surface was adjusted to 50 and 120 μm diameter corresponding to peak fluences of 2.5 and 15 J cm^{-2}, respectively. In order to meet conditions typically applied in imaging systems the focal position was kept above the surface. Since the laser beam showed a Gaussian intensity profile the beam radius r_0 (1/e^2 criterion) had to be determined *via* the energy dependence of the affected area πr_{th}^2. According to Varel,[12] this area can be written as

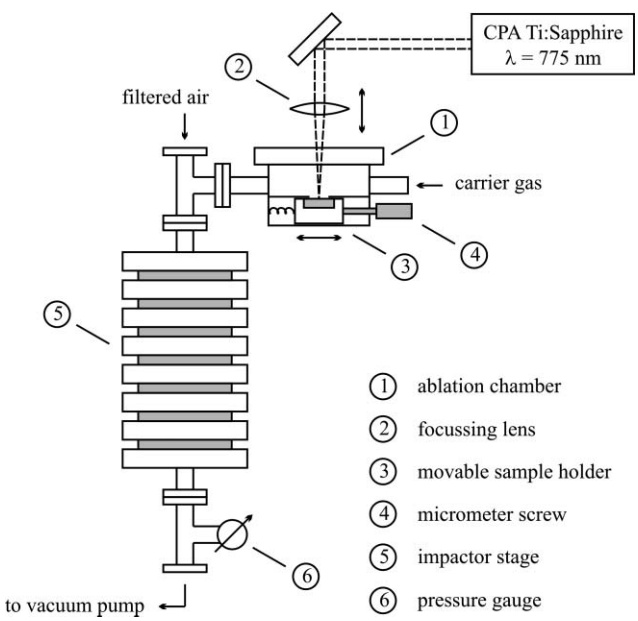

Fig. 1 Experimental arrangement built up for the classification of aerosols produced by nano- and femtosecond LA.

Table 1 Experimental settings typically chosen for aerosol generation by nano- and femtosecond LA and TXRF analysis

Experimental settings	
Aerosol production	
Laser wavelength	775 nm
Pulse duration/energy	170 fs and 5 ns, respectively/300 μJ
Repetition rate	10 Hz
Number of shots per spot	300
Cell design	Cylindrical (V = 20 cm^3)
Flow rate	1 L min^{-1} He or Ar
TXRF analysis	
Extraction/sample volume	250 μL/10 μL (nitric acid)
Internal standard	Se 1000 μg mL^{-1}
X-Ray source/settings	Mo/50 kV, 38 mA
Acquisition time	100 s

$$\pi r_{th}^2 = \frac{\pi r_0^2}{2} \ln F_0 - \frac{\pi r_0^2}{2} \ln F_{th} \quad (1)$$

where F_0 and F_{th} refer to the peak and threshold fluence, respectively.†

Apparently, this expression represents a linear relation on logarithmic scale. Taking into account the proportionality of pulse energy and peak fluence, r_0 can be derived from the slope if E is plotted against πr_{th}^2. Please note, that additional evaluation of the axis intercept enables to determine the threshold fluence, as well, since both F_0 and F_{th} are treated as fitting parameters. The affected area was determined by visual inspection using an optical microscope. In Table 1 the experimental settings are comprehensively listed.

2.2 Aerosol classification and low-pressure impaction

To classify aerosol particles in the micro- and sub-micrometer range optical techniques such as stray light detection (optical particle counting (OPC)) or diffractometry, differential mobility analyses (DMA), and low-pressure impaction can be applied. For classification of laser-produced aerosols, most commonly, OPCs and DMAs are used because of practical reasons. However, the utilization of optical techniques is usually restricted to particle diameters larger than 100 nm whereas DMAs cannot be used above 1 μm. Moreover, these instruments do not provide the feasibility of collecting particles, which is necessary for chemical analyses. In contrast, classification by means of inertial deposition using low-pressure impaction enables to collect particles ranging from about 10 nm up to 10 μm diameter inherently offering the feasibility of chemical analyses.

In the present work, aerosol classification was performed by means of a commercial, 13-stage, low-pressure impactor (DLPI, Dekati, Tampere, Finland) designed for deposition of particles in a range between 30 nm and 10 μm aerodynamic diameter (12 real stages plus 1 stage for separating particles >10 μm). These values are equivalent to physical or so-called Stokes diameters of about 5 nm and 5 μm if brass particles are considered.[13] According to the manufacturer, losses within the impactor are small as long as bounce- and blow-off effects are suppressed and diffusion can be disregarded. However, inter-stage losses due to diffusional deposition in the upper stages can slightly change the actual size distribution and size-dependent composition of the aerosol particles. During operation, a pressure gradient of 900 mbar was applied across the 13 stages (inlet: ambient pressure, first impactor stage: 100 mbar), which resulted in a total throughput of 10 L min^{-1}. However, since the flow rate of the aerosol carrier gas was restricted to 1 L min^{-1} an additional amount of 9 L min^{-1} filtered air was

† Expression (1) results from the damage radius, which is defined by $F_{th} = F_0 \exp(-2r_{th}^2/r_0)$ and refers therefore to the Gaussian fluence distribution at the sample surface.

supplied using a T-type interface connected to the outlet of the ablation cell. The throughput was controlled by means of a pressure gauge positioned behind the last impactor stage.

The aerosol particles were deposited on high-purity polycarbonate membranes (Nuclepore®, Corning, Bodenheim, Germany), which were fixed onto each collection plate. In order to prevent bounce- and blow-off effects during separation the membranes were pre-treated using a minor quantity of pure Vaseline®.

2.3 Extraction procedure and TXRF analysis

Because of the small amount of material deposited in individual impactor stages, a sensitive method with low sample need had to be applied for element-selective quantification. These conditions are met by TXRF analysis.[14]

Loaded filters were carefully removed from the impactor stages by means of nylon tweezers and deposited into small Eppendorf® containers (Micro Test Tubes 3810, 1.5 mL). In a first step, 250 μL of HNO_3 Suprapur® grade from Merck were added to each filter. Subsequently, an internal standard in form of diluted acid solution of a Se single element certified stock standard of 1000 μg mL^{-1} (Alfa Products, Johnson Matthey, Karlsruhe, Germany) with a final mass of 25 ng Se was added to each filter. The containers were thoroughly shaken for 1 min at room temperature using a commercial shaker (REAX 2000, Heidolph, Germany). After 15 min shaking was repeated. An aliquot of 10 μL was taken from the final solution and pipetted onto quartz glass sample supports for TXRF. The acid was evaporated by means of an IR lamp and the obtained residues were analysed.

A commercial TXRF instrument (EXTRA II, R. Seifert & Co, Ahrensberg, Germany) equipped with Mo and W X-ray tubes and a Si(Li) detector/analyser system (QX 2000, Link System, Oxford Instruments, High Wycombe, UK) was used. Analyses were performed by irradiating the samples using a Mo X-ray tube applying 50 kV and up to 38 mA. The acquisition time was mostly set to 100 s. Only in cases of very small sample quantities 200 s were chosen. The element masses of collected particles were determined by taking into account the mass of the internal standard added as usual in TXRF. The quantification limits for the two elements in question, Cu and Zn, are in this particular case about 200 pg. Measurement uncertainties are of the order of 3–10% of relative values depending on the elements, on the acquisition time, and the masses to be analysed. The uncertainty increases up to about 40% when working close to the detection limits.

3 Results and discussion

Primary particle size distributions of aerosols can only be measured by impaction if material losses during transportation due to diffusion, gravitational settling and inertial deposition, are negligible. Assuming the main mass of the primary aerosol being located in a size range below 100 nm, in fact, these transportation losses can completely be disregarded provided that the transport distance is kept well below 1 m (see discussion in section 3.4). Another precondition for achieving high transport efficiencies is to avoid material deposition due to direct contact of the expanding aerosol with the inner wall of the ablation cell. According to Arnold *et al.*[15] typical stopping distances of expanding aerosols are of the order of a few mm under atmospheric conditions. Therefore, cell volumes significantly larger than 1 cm^3 can be regarded as uncritical as long as the anisotropic character of aerosol expansion is taken into account, *i.e.* the distance between the sample and the quartz window is kept well above the stopping distance. In order to circumvent this problem the volume and dimensions of the ablation cell used in the present work were carefully chosen.

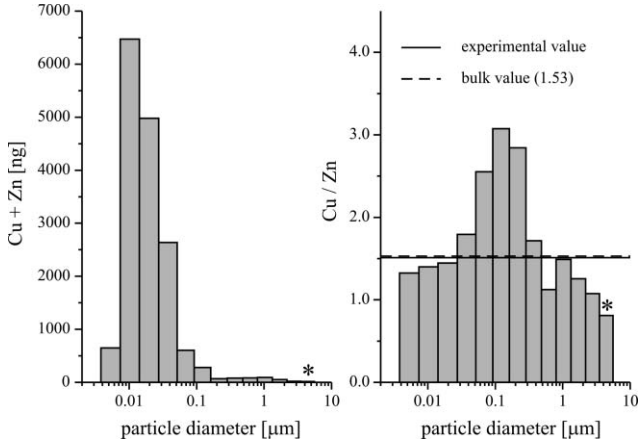

Fig. 2 Particle size distribution and composition determined for femtosecond LA under He atmosphere and a fluence of 2.5 J cm^{-2} (total number of shots: 1.5×10^4). The 13th fraction indicated by an asterisk acts as a separator for particles >3.5 μm.

3.1 Femtosecond laser ablation

In the left part of Fig. 2 a typical mass distribution of aerosols produced by femtosecond LA of brass applying a moderate fluence of 2.5 J cm^{-2} and He as as carrier gas is shown. As can be seen, an ultra-fine, monomodal aerosol was generated under these conditions. On the basis of a non-linear regression (log–normal fitting function), the mean diameter and peak width of this distribution were determined to $d_p \approx 10$ nm and $w_p \approx 35$ nm, respectively. The relative mass fraction of particles larger than 100 nm was less than 5%. For Ar this value was found to be slightly higher (about 15%). Moreover, the mean diameter of the aerosols was shifted towards larger values ($d_p \approx 40$ nm). It is interesting to note that the individual, *i.e.* size-dependent Cu/Zn ratio strongly varied. Smaller particles were Zn-enriched whereas larger particles tend to accumulate Cu, as can be seen in the right part of Fig. 2. However, taking into account all particles impacted, the total Cu/Zn ratio (solid line) corresponded to the original sample composition (dashed line), independent on the carrier gas chosen. Typical deviations were only in the range of 3–5%. The size-dependency of the Cu/Zn ratio could be reproduced within the limits of experimental uncertainty (about 15%) and turned out to be characteristic for both femto- and nanosecond LA (see below).

In contrast to the low fluence regime, ablation at larger fluences resulted in the formation of polydisperse, bimodal aerosols. For example, LA at a fluence of 15 J cm^{-2} produced particles, which were distributed around $d_{p1} \approx 20$ nm ($w_{p1} \approx 50$ nm) and $d_{p2} \approx 1$ μm ($w_{p2} \approx 5$ μm) (see Fig. 3). Therefore, the relative mass fraction of particles larger than 100 nm was drastically increased and amounted to 38% for He and 51% for Ar. Nevertheless, the total Cu/Zn ratio was still in acceptable agreement with the composition of the bulk material.

3.2 Nanosecond laser ablation

In order to examine the influence of the pulse duration on particle size distributions and compositions, comparative measurements were performed using nanosecond LA. The experimental parameters were set to the same values chosen above, *i.e.* aerosols were generated under He as well as Ar atmosphere applying fluences of 2.5 and 15 J cm^{-2}, respectively. A typical size distribution for LA under Ar atmosphere is shown in Fig. 4. Apparently, the size distribution of this aerosol totally differed from those shown in Figs. 2 and 3, in particular, with respect to the percentage of particles above a diameter of 100 nm. The relative mass fraction of these particles even exceeded 65% for high fluences (see Table 2). In contrast, the application of He as carrier gas generally resulted

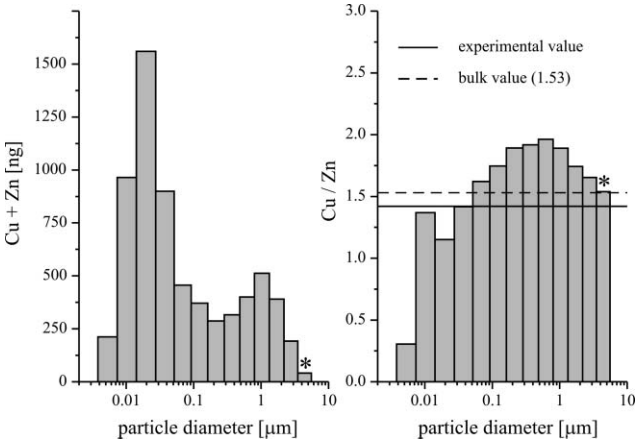

Fig. 3 Particle size distribution and composition determined for femtosecond LA under He atmosphere and a fluence of 15 J cm^{-2} (total number of shots: 1.5×10^4). The 13th fraction indicated by asterisk acts as a separator for particles >3.5 μm.

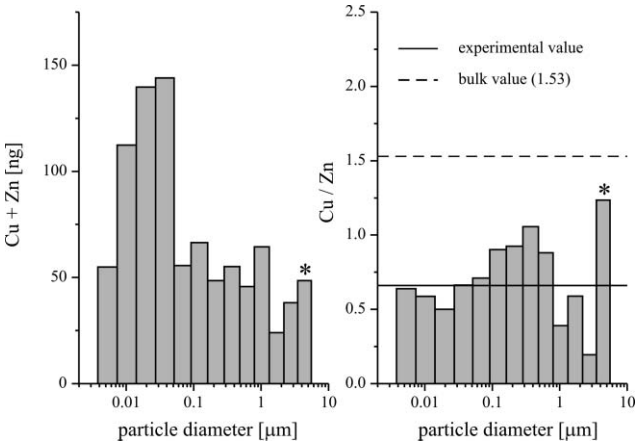

Fig. 4 Particle size distribution and composition determined for nanosecond LA under Ar atmosphere and a fluence of 2.5 J cm^{-2} (total number of shots: 1.5×10^4). The 13th fraction indicated by asterisk acts as a separator for particles >3.5 μm.

in the formation of bimodal aerosols, similar to femtosecond LA applying high fluences. However, the percentage of larger particles was slightly increased in this case (about 20%), as shown in the right part of Fig. 5.

Depending on the carrier gas used the total Cu/Zn ratio of

Table 2 Characteristic data for particle size distributions and compositions aerosols produced under varying conditions. The data are based on a non-linear least-squares fit using a log-normal fitting function

	Fluence/ J cm^{-2}	Mean particle diameter[a]/ nm	Peak width/ nm	Particle mass above 100 nm (%)	Deviation from bulk Cu/Zn ratio (%)
Femtosecond LA					
He	2.5	15	33	4.3	−2.6[d]
	15[b]	20	50	38	−7.2
Ar	2.5	36	53	18	+0.7[d]
	15[b]	<10	24	51	+16
Nanosecond LA					
He	2.5[b]	13	20	17	−27
	15[b]	16	39	47	−12
Ar	2.5	21	58	43	−57
	15[c]	<10	30	66	−22

[a] In the case of bimodal aerosols the first maximum was evaluated. [b] Pronounced bimodality observed. [c] Multimodality not determinable due to restricted size range. [d] Is in agreement with the bulk composition within the estimated experimental uncertainty (±3–7%)

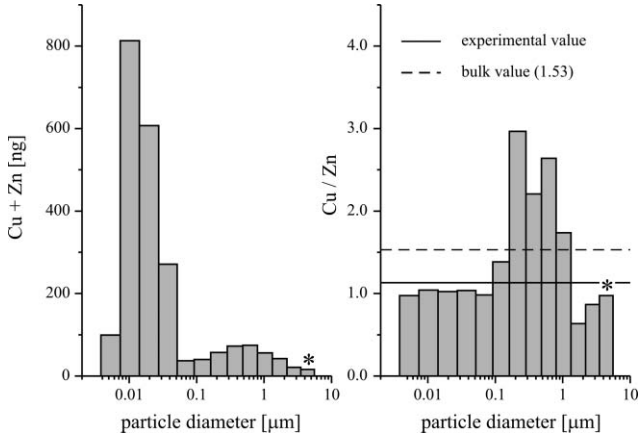

Fig. 5 Particle size distribution and composition determined for nanosecond LA under He atmosphere and a fluence of 2.5 J cm^{-2} (total number of shots: 1.5×10^4). The 13th fraction indicated by asterisk acts as a separator for particles >3.5 μm.

the aerosols deviated up to a factor of about two from the real sample composition indicating strong fractionation during the ablation process. Furthermore, the over-all mass impacted was strongly reduced, which suggested substantial losses of larger particles during the transport period due to gravitational settling and inertial deposition. As a result, nanosecond LA resulted in a mass yield, which was smaller by about one order of magnitude compared to the femtosecond case applying the same number of shots. It is can therefore be assumed that for those aerosols shown in Figs. 3–5 deviations from the expected Cu/Zn ratio are additionally intensified by selective losses of micrometer particles. In Table 2, the characteristic data (mean diameter, peak width, modality *etc.*) of all aerosols classified in the present work are comprehensively listed.

It is interesting to note that according to Jaworski *et al.*[16] the formation of bimodal aerosols can also be observed for nanosecond LA in the near UV (λ = 355 nm) if the number of shots per spot is kept sufficiently small (below approximately 1000). This result is in agreement with preliminary measurements carried out in our laboratory using the fourth harmonic of the Nd:YAG (λ = 266 nm).

3.3 Fundamental considerations

Several mechanisms potentially relevant for aerosol formation during the ablation process using different pulse durations have been discussed in the literature during recent years. These include, for instance, nucleation and particle re-condensation from supersaturated vapor,[17] phase explosion,[17] and critical-point phase separation[18] whereby the latter is merely discussed in the context of femtosecond LA. Though no direct experimental evidence has been reported in the literature, particle re-condensation is usually assumed to be the most important mechanism for nano- as well as femtosecond LA. However, due to fast plasma expansion, the duration of this process should be stopped after a couple of microseconds. As a result, the mean diameter of particles grown from supersaturated vapor should be restricted to a few tens of nanometer as indicated, *e.g.*, by Luk'yanchuk *et al.*[19]

Obviously, the mean particle diameter of most aerosols classified in the present work is well below 100 nm implying that nucleation and particle re-condensation can be assumed as the dominant mechanisms since there is no other process known leading to the formation of such small particles only. However, for those aerosols shown in Figs. 3–5, a different or at least coexistent mechanism has to be taken into account as particles significantly larger than 100 nm cannot be formed by re-condensation due to the high cooling rate of the expanding plasma which is of the order of 10^{11} K s^{-1}.[19] Coexisting

processes, that can result in the formation of larger particles are, for instance, splashing due to hydrodynamic instabilities, coalescence, or plasma–wall-interactions. In contrast, phase explosion, *i.e.* the explosive-like relaxation of a supercritical liquid could, in principle, act as a single source for both smaller and larger particles as it produces a mixture of droplets and vapor. However, as stated above the existence of these processes is still subject to controversy and has to be verified by additional experimental investigations.

3.4 Transport properties of laser-produced aerosols

As already mentioned above, transport- and ICP-induced fractionation phenomena are strongly correlated if the aerosol is subject to selective, *i.e.* size-dependent losses during the transport as a result of diffusion, gravitational settling, and inertial deposition. For ultra-fine aerosols which are produced by near-IR femtosecond LA at low fluences, gravitational and inertial losses can obviously be neglected because of the minor particle mass. Therefore, transport-induced fractionation can only arise if particles underlie heavy diffusion to the inner walls of the transport tube. According to Gormley and Kennedy,[20] the over-all losses within a cylindrical tube caused by diffusion are given by

$$\eta = 1 - 0.819e^{-3.657\xi} - 0.097e^{-22.3\xi} - 0.032e^{-57\xi} \quad (2)$$

for $\xi > 0.02$ and

$$\eta = 2.56\xi^{2/3} - 1.2\xi - 1.77\xi^{3/4} \quad (3)$$

for $\xi < 0.02$ with $\xi = lk_BT/(3\dot{V}vd_p)$.

Here l denotes the tube length, T the gas temperature, $\dot{V}$ the flow rate, v the viscosity, and d_p the particle diameter. Taking into account a mean particle diameter between 5 and 50 nm the losses are smaller than 2% even for transport distances of 1 m (see Fig. 6). Therefore, primary aerosols should remain nearly unchanged under those conditions.

To prove this hypothesis, the total transport efficiency was determined for aerosols produced by femtosecond LA under He atmosphere (low fluence case). For this purpose, the ablated mass (crater volume) was measured using a white light interferometer (New View 5000, Zygo, Middlefield, USA) and subsequently compared with the particle mass impacted. Taking into account the experimental uncertainty associated with the measurement of crater volumes it was found that at least 90% of the mass ablated was deposited on the collection plates of the impactor.

However, as suggested in section 3.2, losses due to gravitational settling and inertial deposition cannot be disregarded if the aerosol under investigation consists of a larger fraction of micrometer particles as was observed for nanosecond LA and femtosecond LA at high fluences. Under such conditions the measured particle size distribution of micrometer particles may differ from those of the primary aerosol since losses of larger particles within the cell and on the way to the impactor must be taken into account. For instance, a considerable amount of large particles could be observed on the sample surfaces around the craters by REM. Therefore, it was not surprising that masses found in the impactor significantly deviated from those determined by interferometric measurements of craters produced by nanosecond LA.

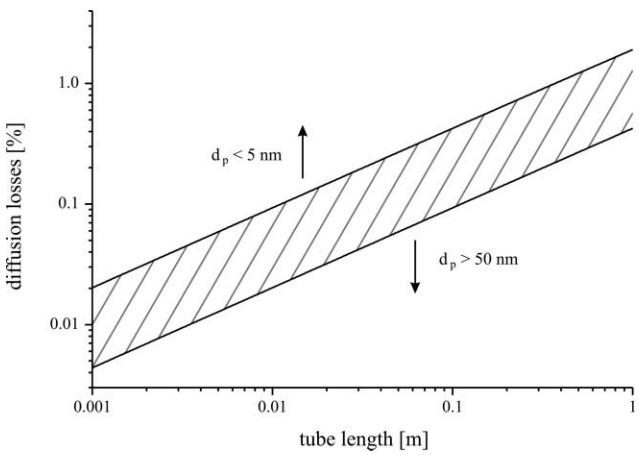

Fig. 6 Calculated diffusion losses of particles with a diameter between 5 and 50 nm as a function of the transport distance assuming a flow rate of 1 L min^{-1}.

3.5 Analytical implications

Indispensable preconditions for an accurate analysis of solid samples by LA-ICP spectrometry is the generation of aerosols which (i) reflect the composition of the bulk material and (ii) can be transported over distances typically used in LA-ICP arrangements ($\approx$1 m). The results documented above indicate that near-infrared femtosecond LA carried out at moderate fluences of 2.5 J cm^{-2} apparently meets these requirements, independent on the carrier gas chosen. However, at fluences larger than 10 J cm^{-2} femtosecond LA results in the intensified formation of particles in the micrometer range. From an analytical point of view, these conditions are less favorable since particles in the micrometer range can give rise to ICP-induced fractionation (incomplete vaporization), as indicated by Guillong and Günther.[11]

In contrast, nanosecond LA generally intensifies the production of particles with diameters >100 nm. This is, however, less pronounced for LA in He. Furthermore, the Cu/Zn ratio of aerosols produced by near-IR nanosecond LA was found to strongly deviate from the bulk value.

4 Conclusions

The present work reported on the element-selective analysis of brass aerosols produced by near-IR nano- and femtosecond LA at atmospheric conditions using low-pressure impaction and TXRF analysis. It was demonstrated, that femtosecond LA of brass carried out at moderate fluences generally results in the generation of ultra-fine (mean diameter $d_p \approx 10$ nm), monomodal aerosols, which in total reflect the composition of the bulk material. In contrast, nanosecond LA leads to an increased formation of particles in the micrometer range which is, however, less pronounced for LA under He atmosphere. The Cu/Zn ratio of these aerosols strongly departs from the bulk composition, implying that near-IR nanosecond LA at atmospheric pressures has to be regarded as critical for the analysis of metals. A size-dependent analysis of the Cu/Zn ratios moreover revealed that for nano- as well as femtosecond LA the small particles are generally Zn-enriched whereas larger particles tend to carry more Cu.

According to the hydrodynamic properties of ultra-fine aerosols it can furthermore be assumed that losses due to diffusion, gravitational settling, and inertial deposition are negligible. As a result, such aerosols should be (i) transportable without significant losses and (ii) sufficiently fine to be atomised within the ICP. The latter statement certainly represents a hypothesis since it merely rests upon the atomisation cut-off diameter typically found for dielectric particles.[11] Future investigations should critically prove this statement.

The intensified production of micrometer particles observed for nanosecond LA possibly indicate differences to the femtosecond case concerning the formation of particles under similar conditions. However, it should be emphasized, that in the present work the laser fluence was varied by means of beam defocusing instead of attenuating. Consequently, an

influence of the spot size on the formation of larger particles cannot generally be excluded. Another parameter recently identified to drastically increase the relative amount of micrometer particles during nanosecond LA is the number of shots applied or crater depth, respectively.[16] However, to get further insight into these processes additional measurements involving different spot sizes, matrices (conductive as well as non-conductive materials), laser wavelengths, aspect ratios, *etc.*, have to be performed. From an analytical point of view, such investigations are important to specify optimum conditions for suppressing laser-induced fractionation and thus to improve the accuracy of non-matrix-matched analyses by LA-ICP spectrometry.

First measurements dealing with the aerosol production by nanosecond LA at 266 nm have already been performed. According to our results deviations of the total aerosol composition from the bulk stoichiometry were less pronounced compared to nanosecond LA at 775 nm ($\leqslant 10\%$). However, it has also been observed that the formation of micrometer particles could not sufficiently be suppressed even if ablation was carried out under He atmosphere.

Acknowledgements

Active help in the experiment by M. Becker, H. Lindner and N. Ahlmann is gratefully acknowledged.

References

1 S. F. Durrant, *J. Anal. At. Spectrom.*, 1999, **14**, 1385.
2 H. P. Longerich, D. Günther and S. E. Jackson, *Fresenius J. Anal. Chem.*, 1996, **355**, 538.
3 K. Niemax, *Fresenius J. Anal. Chem.*, 2001, **370**, 332.
4 R. E. Russo, X. Mao, H. Liu, J. J. Gonzalez and S. S. Mao, *Talanta*, 2002, **57**, 425.
5 X. Mao and R. E. Russo, *J. Anal. At. Spectrom.*, 1997, **12**, 177.
6 C. Pickhardt, J. S. Becker and H.-J. Dietze, *Fresenius J. Anal. Chem.*, 2000, **368**, 173.
7 J. Koch, I. Feldmann, N. Jakubowski and K. Niemax, *Spectrochim. Acta, Part B*, 2002, **57**, 975.
8 H. R. Kuhn and D. Günther, *Anal. Chem.*, 2003, **75**, 747.
9 R. E. Russo, X. Mao, J. J. Gonzalez and S. S. Mao, *J. Anal. At. Spectrom.*, 2002, **17**, 1072.
10 P. M. Outridge, W. Doherty and D. C. Gregoire, *Spectrochim. Acta, Part B*, 1996, **51**, 1451.
11 M. Guillong and D. Günther, *J. Anal. At. Spectrom.*, 2002, **17**, 831.
12 H. Varel, *Untersuchungen zur Ablation dielektrischer Materialien mittels Ultrakurzpulslaser*, PhD thesis, Free University of Berlin, 1999.
13 K. Willeke and P. A. Baron, *Aerosol measurements*, Van Nostrand Reinhold, New York, 1993.
14 R. Klockenkämper and A. von Bohlen, *J Anal. At. Spectrom.*, 1992, **7**, 273.
15 N. Arnold, J. Gruber and J. Heitz, *Appl. Phys. A*, 1999, **69**, 87.
16 R. Jaworski, E. Hoffmann and H. Stephanowitz, *Int. J. Mass Spectrom.*, 2002, **219**, 373.
17 D. Bäuerle, *Laser Processing and Chemistry*, Springer-Verlag, Berlin–Heidelberg–New York, 3rd edn., 2000.
18 F. Vidal, T. W. Johnston, S. Laville, O. Barthelemy, M. Chaker, B. Le Drogoff, J. Margot and M. Sabsabi, *Phys. Rev. Lett.*, 2001, **86**, 2573.
19 B. S. Luk'yanchuk, W. Marine and S. I. Anisimov, *Laser Phys.*, 1998, **8**, 291.
20 P. Gormley and M. Kennedy, *Proc. R. Irish Acad.*, 1949, **52**, 163.